Supporting Information: Replicating programmed colloidal sequences

Steven van Kesteren, Pascal Diethelm, Lucio Isa

May 4, 2023

Contents

1 Extended Materials & Methods

A schematic overview of the primary experiments is shown in Figure S1. The following sections will describe the experimental methods.

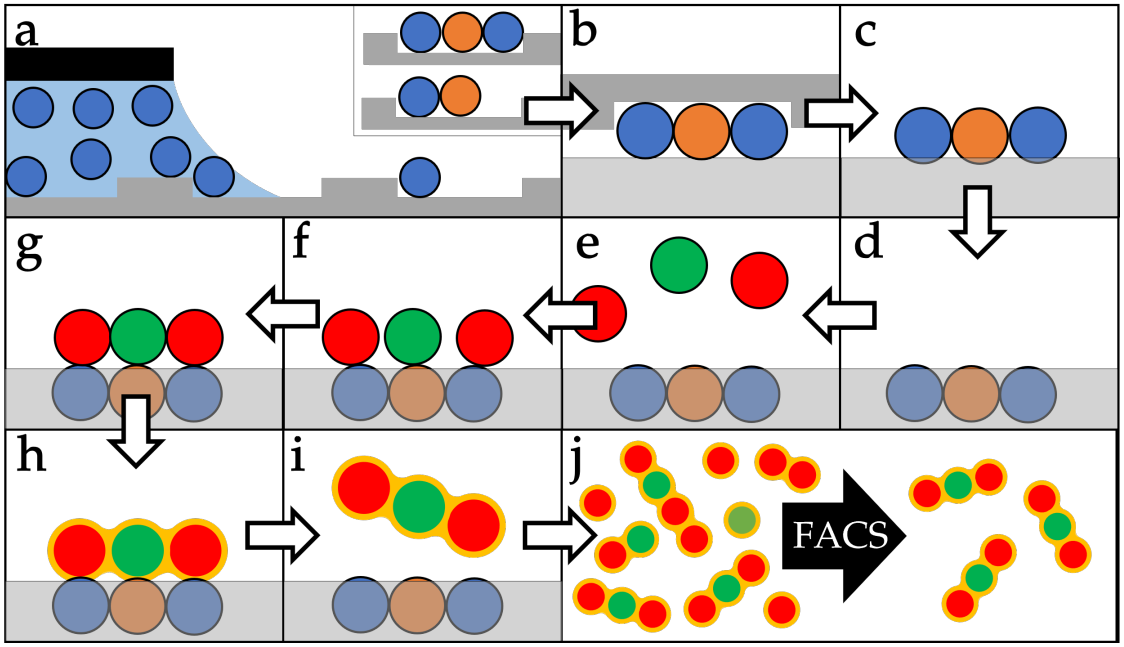

Figure S1: (a) Production of primer particle sequence by sCAPA. (b),(c) Transfer of the colloids from the sCAPA template to a polymer-coated glass slide. (d) Embedding of the primer colloids into the polymer. (e) Addition of the complementary colloids. (f) The complementary colloids bind specifically to the template colloids. (g) The complementary colloids are aligned using a magnetic field. (h) The complementary colloids are cross-linked using polyelectrolytes. (i) The complementary colloids are released using mechanical vibration. (j) FACS sorting of the harvested colloids.

1.1 DNA-functionalization

The functionalization of colloids with DNA is schematically summarized in Figure S2.

1.1.1 Streptavidin-modification of silica colloids

Silica colloids were functionalized with streptavidin (STV) using the following procedure adapted from literature [1], and as reported in a previous work [2]. In short, silica colloids were coated with APTES, glutaraldehyde, and then STV. Specifically, 0.5 ml 5 % w/w silica colloids were washed three times with Milli-Q water. Then, 0.5 ml hydrogen peroxide 30% w/w (Sigma-Aldrich) and ammonia 25% w/w (Sigma-Aldrich) was added and heated to 70 °C for 10 minutes to clean and activate the silica surfaces. Then the particles were washed three times with 1 ml Milli-Q and three times with 1.5 ml dry ethanol (Sigma-Aldrich, >99.8 %). Then 70 µl of APTES (ACROS, 99%) was added to the particles suspended in dry ethanol and gently mixed for 16 h. The APTES-modified particles were washed three times with 1.5 ml ethanol, and three times with 1 ml phosphate-buffered saline (PBS), and resuspended in 1 ml PBS with 0.1 % w/w Pluronic F127. 1 ml glutaraldehyde 25% v/v (Sigma-Aldrich) was added to 0.5 ml of this suspension and

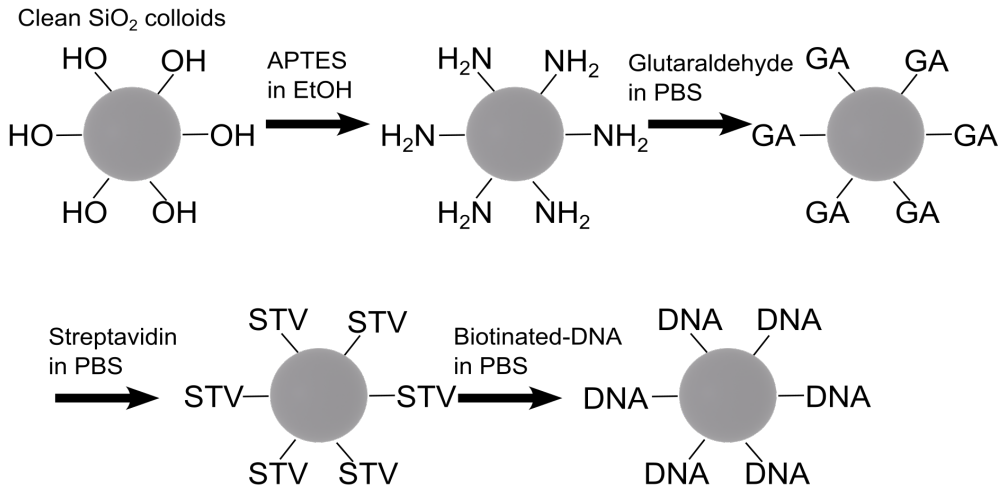

Figure S2: Schematic of the DNA functionalization procedure of SiO_2 colloids.

gently mixed on a rotary stirrer for 3 h. After the 3 h, a slight discoloration of the glutaraldehyde was observed. The glutaraldehyde-modified particles were cleaned five times with 1 ml PBS + Pluronic and subsequently 100 µl 2 mg/ml streptavidin (Apollo Scientific, 97%) in PBS was added. The reaction proceeded for 16 h under gentle mixing and then the particles were cleaned three times with 1 ml hybridization buffer (50 mM phosphate, 50 mM NaCl). Finally, the particles were suspended in 1 ml of buffer (50 mM phosphate, 50 mM NaCl buffer with 0.001% w/w NaN3) for storage, with a final particle concentration of 2.5% w/w (not accounting for losses due to washing).

1.1.2 DNA functionalization of streptavidinated colloids

The DNA functionalization protocols were adapted from literature [3]. The DNA-sequences are shown in Table S1 below and were purchased from Microsynth AG.

Table S1: DNA sequences of the different strands with the sticky ends underlined.

A (green)	5'-GCACCT TTTTT ACGAGATTGAAGACCCTGGATGGAGAGACGGAGCGAAGTAACC-Atto488-3'
A' (orange)	5'-AGGTGC TTTTT ACGAGATTGAAGACCCTGGATGGAGAGACGGAGCGAAGTAACC-Cy3-3'
B (red):	5'-TTGCCG TTTTT ACGAGATTGAAGACCCTGGATGGAGAGACGGAGCGAAGTAACC-Cy5-3'
B' (blue):	5'-CGGCAA TTTTT ACGAGATTGAAGACCCTGGATGGAGAGACGGAGCGAAGTAACC-Atto425-3'
Backbone:	5'-Biotin-TTTTT GGTTACTTCGCTCCGTCTCTCCATCCAGGGTCTTCAATCTCGT-3'

First, the fluorescent "sticky ended" DNA (A, A', B, or B') was hybridized with biotinylated

backbone DNA by mixing 25 µl "sticky ended" DNA (100 µM in TE-buffer, 10 mM Tris(Sigma) + 1 mM EDTA (Sigma)), with 25 µl backbone DNA (100 µM in TE-buffer), with 200 µl hybridization buffer (50 mM phosphate pH 7.4, 50 mM NaCl). To ensure well-equilibrated biotinylated double-stranded DNA, the DNA mix was then heated to 90 °C and let slowly cool down to RT for approximately 3 h in an Eppendorf incubator. This DNA mix was stored in the fridge for up to 2 months. Subsequently, particles were coated with DNA by mixing 50 µl STV-modified particle suspension (2.5 % w/w for the silica colloids and 1% w/w for the Dynabeads M270), 25 µl double-stranded DNA-mix and 425 µl hybridization buffer (50 mM phosphate, 50 mM NaCl), in a rotary mixer for 16 h. The DNA-functionalized colloids were washed three times with suspension buffer (10 mM phosphate pH 7.4, 50 mM NaCl, 0.5 % w/w Pluronic F127(Sigma-Aldrich,99 %)), and concentrated in 250 µl or 100 µl suspension buffer, for the silica colloids and Dynabeads, respectively. This resulted in a final particle concentration of 0.5% w/w.

1.2 sCAPA

The negatives for the traps for sCAPA were prepared on Si wafers. For this, a SU-8 pattern was written on a standard Si wafer using a Nanoscribe Photonic Professional GT2 following an in-house procedure. In short, a 1 µm film of SU-8 6001-TF was prepared by spin coating on a plasma-cleaned 4-inch Si wafer (30 s, 2000 rpm). The film was pre-baked on a 110 °C hot plate for 3 min. Then, the pattern was written on the wafer using a Nanoscribe Photonic Professional GT2 with a 20x objective (laser power 75 %, writing speed 10000 µm s$^{(}$-1), two passes). After exposure, the wafer was baked at 110 °C for 2 min and then developed in PGMEA for 3 minutes and rinsed with PGMEA and IPA. The finished wafer was hard-baked for 1.5 h at 175 °C. Subsequently, chemical vapor deposition was then carried out by placing the developed wafer in a vacuum chamber containing approximately $50\,\mu$L of trichloro(1H,1H,2H,2H-perfluorooctyl)silane (Sigma-Aldrich, > 98%) for 30 minutes.

Before use, the wafer was rinsed with ethanol and then dried with dry N_2. Then, a PDMS silicon-based elastomer (Dow Chemicals' SYLGARD 184 silicone elastomer) was poured over the silicon wafer and left to cure overnight at 80 degrees C to complete the PDMS template preparation. The suspension for the sCAPA was freshly prepared before each deposition. The surfactant concentration of the sCAPA suspension was optimized to give the right contact angle for single particle deposition [4]. The final suspension contained 0.015 % w/w colloids in 10 mM NaCl, 50 mM phosphate pH 7.4, 2 mM sodium dodecyl sulfate (Sigma-Aldrich), and 0.02 % v/v Triton X-45 (Sigma-Aldrich). Per deposition, $45\,\mu$l was used, and the droplet was moved over the substrate at $7\,\mu\mathrm{m/s}$. To ensure that the subsequent deposition did not remove the deposited colloids, the PDMS template with colloids was heated to 130 °C for 45 s between each deposition. The sCAPA samples were used within 24 h.

1.2.1 Transfer and sink-in

For the transfer, $0.17\,\mathrm{mm}$ glass slides were cleaned with IPA. For the coating with PS, the slides were directly used after cleaning, while for the PMMA, the glass slides were first treated by placing them in a vacuum chamber with approximately $50\,\mu$l 3-(trimethoxysilyl)propyl methacrylate (Sigma-Aldrich, ¿98%) for 16h and subsequently cleaned with ethanol. 40 w/w % PMMA (15 kDa) or PS (35-40 kDa) was dissolved in PGMEA and spin-coated at 4000 rpm for 30 s on the glass slides. To evaporate the PGMEA and anneal the polymer, the coated glass slides were placed on a hot plate for 60 min at 120 °C, 20 minutes at 160 °C, and 10 min at 200 °C. For the transfer, the sCAPA template with the deposited colloids was placed with the colloids facing toward the polymer-coated glass slide and placed for $20\,\mathrm{s}$ on a hot plate at 110 °C for PS and 120 °C for

PMMA. The sink-in was done by placing the glass slide with the transferred colloids on the hot plate for 15 s at various temperatures, typically at 140 °C for the PS samples unless mentioned otherwise.

1.3 Microfluidic chip design and experimental set-up

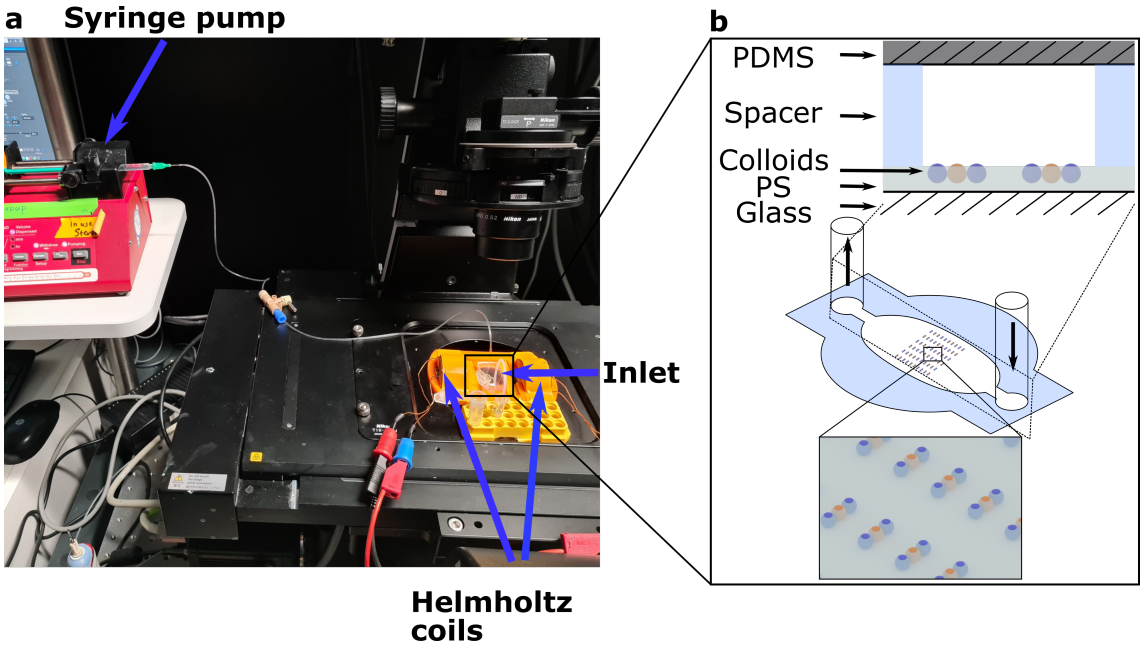

Figure S3: **Microfluidic chip design** a) Photograph of the experimental binding set-up on an inverted microscope (Nikon, Eclipse TI-2), with all the important components annotated. b) Schematic overview of the microfluidic chip design, showing a cross-section of the different layers (relative thicknesses not to scale).

We assembled the microfluidic device for the binding experiments using the following steps: First, we sank the colloids into the PS layer as described above, then we placed a pre-cut spacer with a thickness of 120 µm on top of the sample. We used a Silhouette Cameo 4 cutting plotter to cut the spacers into the desired shape. Next, we attached a plasma-treated PDMS piece, with a thickness of approximately 1 cm and two access holes, onto the spacer. We bonded the sample on a hot plate for 1 min at 120 °C. After that, we fitted tubes into the PDMS roof, with one long Tygon tube connected to a syringe pump and the other shorter PTFE tube placed in an Eppendorf. The cell was then mounted on the microscope (Nikon, Eclipse Ti-2) and connected by tubings to the syringe pump.

Additionally, the chip was placed between two hand-made Helmholtz coils with steel cores mounted on a custom 3D-printed holder. These coils could generate a magnetic field up to 14 mT, at 12 V and 3 A. The final set-up is shown in Figure S3.

1.4 Replication experiments

For the initial filling of the cell, the syringe was filled with binding buffer (10 mM phosphate, 250 mM NaCl, 0.5% w/w Pluronic F127), and the solution was pushed through to pre-fill the cell without introducing air bubbles. Afterward, all the solutions and suspensions were pulled in by the syringe pump by placing the inlet tube in the corresponding Eppendorf tube. At first, 3 µl of the complementary monomers (0.05 % A' w/w and 0.05 % w/w in binding buffer) were pulled in

Table S2: Cross-linking and stabilizing process. The reported amounts of polyelectrolyte and solvents were sequentially pulled into the cell at a pump flow rate of 25 µl/min. When flushing with polyDADMAC, a magnetic field was applied.

volume [µl]	**polyelectrolyte**	**medium**
30	-	suspension buffer
30	0.1 wt% polyDADMAC	MilliQ + 0.1 wt% Pluronic F127
30	-	MilliQ + 0.1 wt% Pluronic F127
30	0.1 wt% PSS or 8 nm SiO_2 NPs	MilliQ + 0.1 wt% Pluronic F127
15	-	MilliQ + 0.1 wt% Pluronic F127 c
15	-	binding buffer
30	0.1 wt% PLL-g-PEG	MilliQ + 0.1 wt% Pluronic F127
15	-	binding buffer
15	-	MilliQ + 0.1 wt% Pluronic F127
30	0.1 wt% PSS	MilliQ + 0.1 wt% Pluronic F127
30	-	MilliQ + 0.1 wt% Pluronic F127
200	-	suspension buffer
30	-	MilliQ + 0.1 wt% Pluronic F127

at a rate of 7 µl/min and binding buffer was used for the binding process and the washing. This pulling speed lead to a flow velocity of 9.3 ± 0.7 µm/s. After the particles were bound and washed out, the cross-linking and stabilizing process began. For this, the pump speed was set at 25 µl/min and.

The process is summarized in table S2, showing the sequence of solutions used and schematically shown in Figure S4. When pulling in the polyDADMAC (Sigma-Aldrich, 400-500 kDa), a magnetic field of approximately 14 mT was applied using the Helmholtz coils and afterward switched off. The PSS (polystyrene-sulfonate 70 kDa) was purchased from Sigma-Aldrich and the PLL-g-PEG (poly(L-lysine)-g-poly(ethylene glycol), (20 kDa)-[3.5]-(2)) from SuSOS AG. Between each polyelectrolyte 30 µl of solvents in total were used to wash the cell. After the process was completed, the pump was stopped. The replicated colloids were released by applying mechanical vibration using a toothbrush (Oral-B), without a brush head, by putting it into direct contact with the bottom of the cell for 1-5 s. To harvest the particles, the flow was reversed, and 200 µl were pushed out and collected.

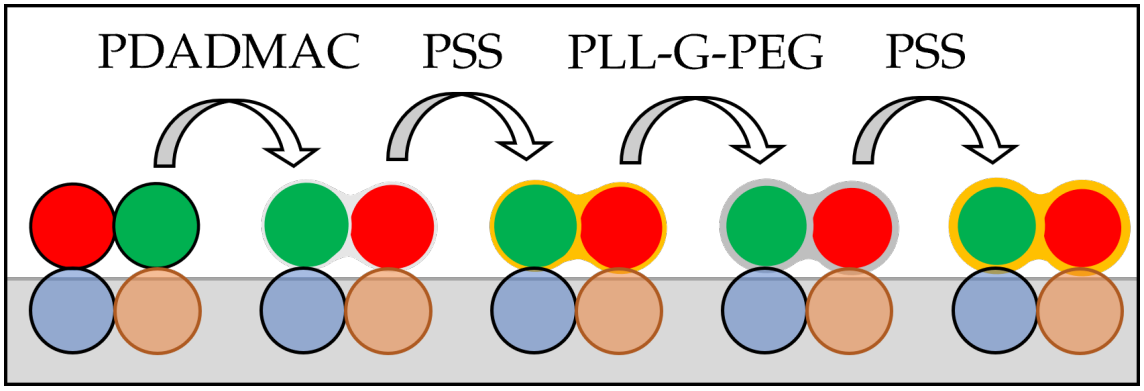

Figure S4: Schematic of the cross-linking and stabilization procedure.

1.5 AFM characterization

In order to characterize the patch area of the particle constituting the primer sequences, we used an atomic force microscope (AFM, Nanosurf NaioAFM, dynamic force mode) to measure the height profile of the protruding patches. Using the freely-available software Gwyddion, any tilt in the background was corrected (Figure S5a). Then from the height profile, the peak height of each particle, and the radius of its protrusion were measured relative to the background (Figure S5). We used three three-particle sequences, therefore nine colloids, to measure the relative patch area A for each temperature, defined as follows:

$$A = \frac{A_{patch}}{A_0} = \frac{2\pi * h_{patch} * r_{patch}}{4\pi * r_0^2} \tag{1}$$

This relative patch area was measured for colloids sunken into PS layers at 105, 120, 140, and 160 °C and PMMA layers at 160, 180, 200, and 220 °C.

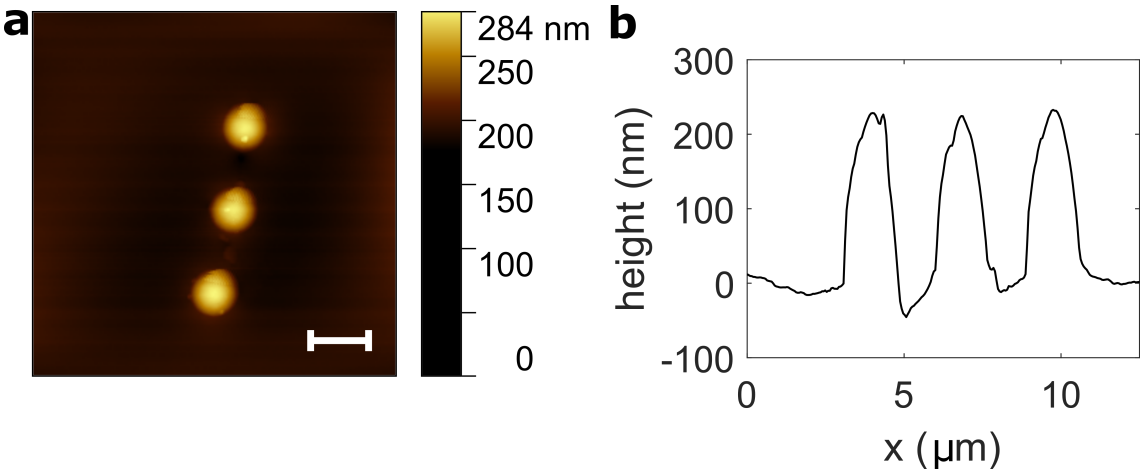

Figure S5: a) An example AFM image of athree -particle sequence embedded in PS at 140 °C. Scale bar is 2 μm. b) Height profile of the colloids from the AFM image shown in a.

1.6 Determine binding angles

The binding angles were calculated from the offset between the center of the particles in the primer sequence and the bound monomer colloids. The binding offsets were determined by binding A' colloids to sunk-in A colloids in a cell, as described in the Replication section. Using a microscope (Nikon, Eclipse Ti-2), the colloids were imaged in various z-planes to focus on the sunk-in A colloid and the bound A' colloids. In a MatLab script, the position of the centers of the A and A' colloids was identified using the in-built imfindcircle function (Circular Hough Transform (CHT) based algorithm for finding circles in images) on two images, one focusing on A and one on A' colloids. Thus, we observed the 2D-projection of the colloids, and from this, we calculate the binding angle ($binding\ angle = sin^{-1}(\frac{binding\ offset}{particle\ diameter})$)

1.7 FACS

At the end of the replication process, the colloidal clusters were sorted by FACS using a BD-FACSAriaIII with a 70 μm nozzle. The colloids were characterized by forward and side scattering and green (502 ex. 530/30 em., ATTO 488) and red (630 ex. 670/30 em) fluorescence lines. For the initial setup, we used the particle suspensions containing only the A' or B' colloids. We used a

first gate on the forward vs. side scattering to select only the two and three-particle clusters. Then on top of this gate, we used secondary gates in the green vs. red fluorescence to select the BAB, BA, and ABA clusters as shown in the main manuscript. The clusters were sorted into Eppendorf tubes containing a 100 µl 0.5 % w/w Pluronic F-127 or directly on a microscope slide and then counted using a fluorescence microscope (Nikon, Eclipse Ti-2).

1.8 Determination of the yield during the various process setps

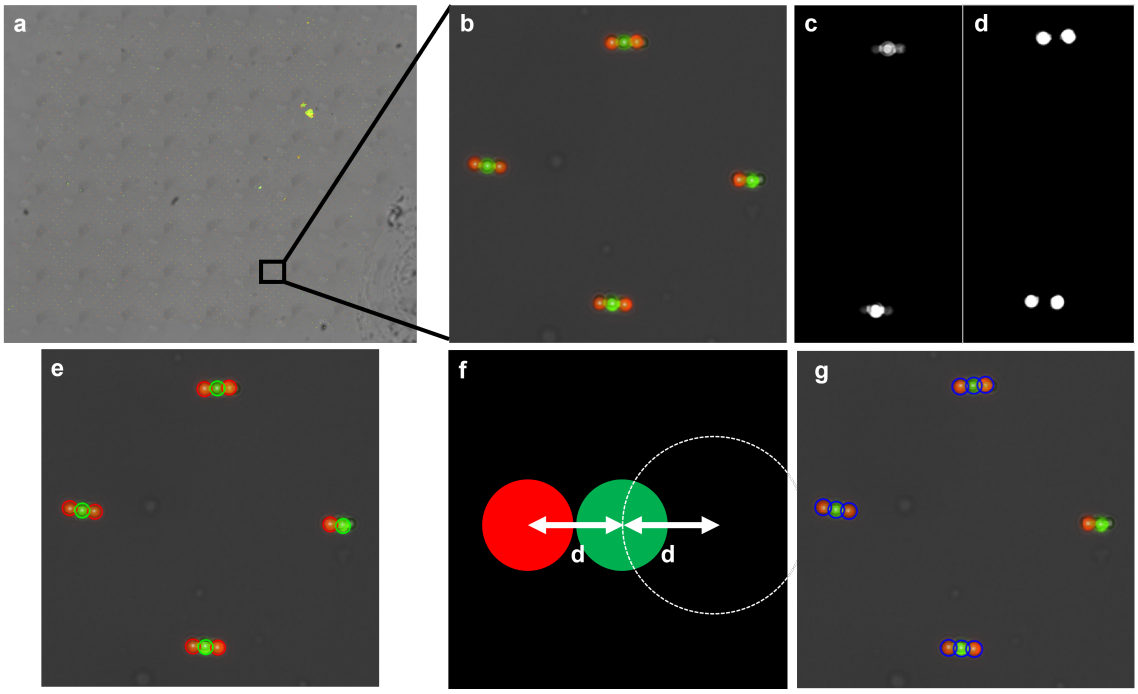

Figure S6: **Method for determining the yield** a) Stitched image of experiment area after crosslinking BAB sequences. b) Zoomed-in image of a). c) Image of GFP (A particle) single channel. d) Image of Cy5 (B particle) single channel e) Tracked particles shown in a fluorescence image. f) Visualization of extrapolation. g) Only the correct target sequences are highlighted in blue.

The yield was determined from microscope images. For this purpose, images of the template were taken after cross-linking and after the release. In each case, an image array was taken and stitched together (Figure S6 a)). Then the various sequences were counted by a MatLab script. The script uses an RGB combined image for illustration (Figure S6 b)) and one single channel image for each particle type of interest (B'/A' for the template, B/A for the others). To facilitate particle detection, contrast and brightness were adjusted (Figure S6 c-d)). The in-built imfindcircle function, a Circular Hough Transform (CHT)-based algorithm for finding circles in images, was used to detect the particles (Figure S6 e)). Before counting the sequences, a first neighbor screening was made. The number of neighbors of a particle was determined by searching for other particles within a given radius. The particles without a neighbor were filtered as they corresponded to monomer colloids. The remaining particles were sorted into particles with one neighbor and particles with more neighbors, increasing the efficiency of the subsequent steps. After that, the combinations of dumbbells were counted (AA, BB, AB). If a one-neighbor particle of one type is found next to another one-neighbor particle within the radius, a particle is considered connected. In the next step, all the linear colloidal sequences were counted. The identification started by

searching for the neighbors of a one-neighbor particle. If this particle was of the correct type and had the correct types of neighbors, the algorithm searched for the third particle around its theoretical position. This position was defined by extrapolating the translation vector between the first and second particle and applying it from the center of the second particle (Figure S6 f)). Upon correct identification, the whole sequence was counted (Figure S6 g). For more particles, the extrapolation step was repeated. In the last step, all the clusters (non-linear particle groups) were counted by searching for groups with neighboring particles and sorted by the group size.

2 Characterization of the DNA-coated colloids

2.1 Number of DNA-strands per colloid

The DNA coverage on the colloids was determined using a binding assay. In this study, we used the absorption of DNA at 260 nm to measure the amount of DNA left in the solution after binding it to a known amount of colloids. We added 0.25, 0.5, and 0.75 mg magnetic Dynabeads and 1.25, 2.5, and 3.75 mg SiO_2 colloids to 200 pmol of the dsDNA and bound it using the standard protocol. We determined the concentration of DNA after binding using a calibration curve (Figure S7a). From this, we used the slope of the number of colloids versus the number of "lost" DNA strands to determine the amount of DNA per colloid (Figure S7b). We measured a DNA coverage of 1.3±0.12 10^6 strands per colloid for the Dynabeads and 4.9±0.23 10^5 strands per colloid for the SiO_2. Additionally, we measured the fluorescence intensity distribution of the colloids with flow cytometry (BD LSRFortessa), and we saw a similar relative brightness between the Dynabeads and the SiO_2 (Figure S7c-d).

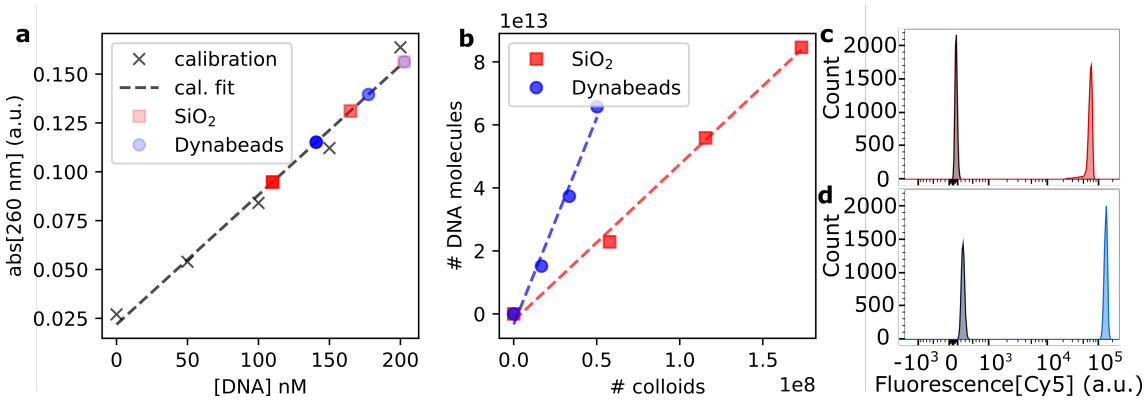

Figure S7: **DNA per colloids** a) Absorption at 260 nm of supernatant after binding with 0, 0.25, 0.5, and 0.75 mg Dynabeads (blue circles), and 0, 1.25, 2.5, and 3.75 mg SiO_2 colloids versus a calibration of 0, 50, 100, 150, and 200 nM DNA "B" (black crosses and dotted line) b) Amount of DNA removed by the sample versus the number of added colloids for the Dynabeads (blue circles), and SiO_2 colloids (red squares), with the fitted slopes indicated with the dotted lines. c-d) Fluorescence distribution of Cy5 measured with flow cytometry for the SiO_2 colloids (c) before (black) and after (red) DNA "B" functionalization, and the Dynabeads (d) before (black) and after (blue) DNA "B" functionalization.

2.2 Melting curve

We determined the melting behavior as follows; We mixed complementary SiO_2 and magnetic colloids in the suspension buffer (see Methods). These colloids were left to aggregate at 22 °C for one h. Subsequently, we placed the sample on a heating stage (Linkam) and slowly heated it at a rate of 0.2 °C min^{-1} and observed the aggregates melting (Figure S8). The heating stage was made from a slightly magnetic metal; thus, magnetic colloids slowly aligned with the field over time. Therefore, we used the diffusivity of the SiO_2 colloids to determine if the particles were aggregated or freely suspended. The diffusivity was extracted by particle tracking using TrackPy [5] and normalized to the diffusion of the free colloids at 50 °C. We then fitted this data with a sigmoid curve ($y = L/(1 + e^{-k(x-x0)}) + b$) to extract the melting point ($x0$) and melting range (k^{-1}).

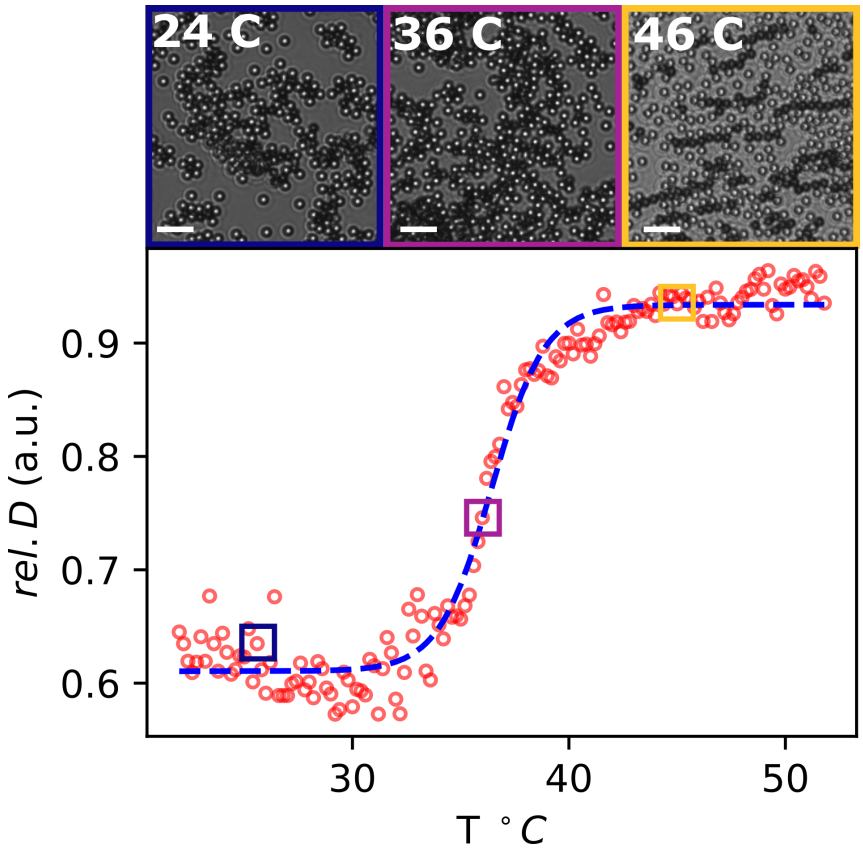

Figure S8: **Melting curve of DNA-coated colloids** The plot shows the mean relative diffusivity of a mixture of A SiO_2 colloids and A' Dynabeads at different temperatures (red dots), fitted with a sigmoid function (blue line). The top panels show a cropped bright-field micrograph corresponding to 24 °C (left), 36 °C (middle), and 46 °C (right). Scale bars are 10 µm.

3 Replication yields

3.1 Spatial variations of the yield

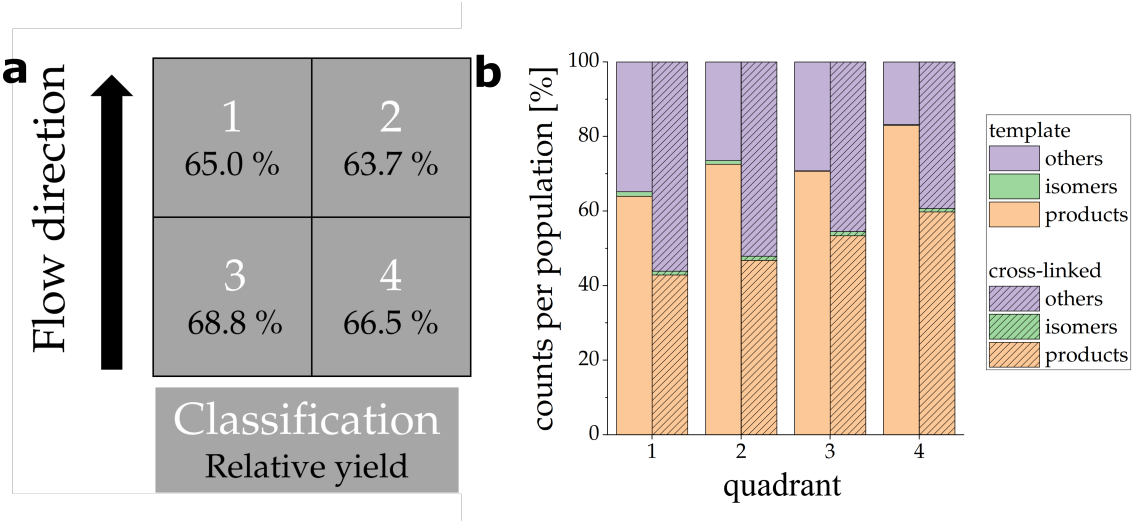

Figure S9: (a) Schematic of the classification and the corresponding replication yields. Scale bars are 20 µm. (b) Relative counts per population for each quadrant on the template (primer) and in the cross-linked state.

To investigate if there were any spatial variations of the yield in our system, the template sequences, i.e., primers, were divided into four quadrants for analysis. In these quadrants, the overall yield of the correct sequences ranged from 64.0 % to 83.0 %. We hypothesize that two main factors influenced these variations. The first one stems directly from the yield of the sCAPA deposition. Depending on the meniscus shape and the number of colloids in the sCAPA solution, the traps on the edges sometimes missed colloids, which led to a lower filling fraction. The second reason is that some residual stresses may have separated the colloids during the transfer, often resulting in a dimer and a single colloid. The range was much smaller if one focused on the relative yield, defined as the number of the correct sequences in the cross-linked state divided by the of correct sequences deposited on the template. This relative yield ranged from 63.7 % to 66.5 %. The two top quadrants of the PDMS template (1 and 2) had a slightly lower yield. Given the direction of the deposition, the suspended particles were already partly consumed when the droplet reaches them S9.

3.2 Yield of cross-linking for silica colloids and cross-linking without a magnetic field

The magnetic field facilitated the cross-linking of the complementary colloids, as it straightened the sequences and snapped them together if the particles were close enough. To quantify the effect of the magnetic field, the process was repeated as described in the Methods, but without applying a magnetic field. Figure S10a shows an image of cross-linked complementary colloids without using a magnetic field. The colloids marked with blue circles were in the right sequence but were not directly in contact, making cross-linking of an entire B'A'B' sequence impossible.

This observation is supported by the decreased share of products (correct sequences) in the cross-linked and released states, as respectively shown in Figure S10b. In the cross-linked state, 21.2 % of products were present, while in the released state, only 8.2 % of the products were

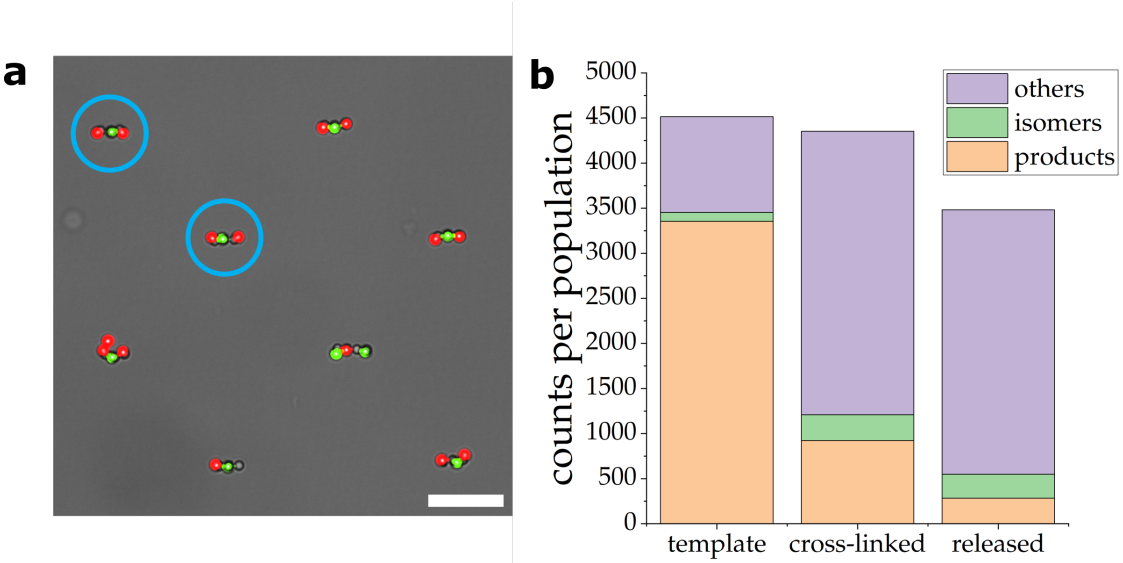

Figure S10: a) Microscope image of the bound B'A'B' sequences without magnetic field. The circles show correct sequences, but where the colloids are not fully in contact. b) Distribution of populations for the template, cross-linked, and released states for BAB magnetic colloids cross-linked without a magnetic field.

present. Usually, the difference between the cross-linked and released states was only 7.7% because of the high cross-linking and release efficiency. But as no magnetic field was applied, many colloids were not touching, so no cross-links could form, and the sequences broke upon release. Compared to results present in the main manuscript with the magnetic field, the isomers in the cross-linked state were taking a 1 % share; without a magnetic field, 6.6 % of isomers were present. The replication yield was 8.5 %, which is only a small fraction of the replication yield when a magnetic field was applied during cross-linking.

As shown in Figure S11, replication with silica colloids is possible. In this case, the same 2.7 um sized silica colloids used for the template were functionalized with the A' and B' DNA. An image of released sequences is shown in Figure S11a. Again, the colloids were counted on the template, in the cross-linked state, and after release, and the results are summarized in Figure S11. The released share of B'A'B' product was at 6 %, and 5 % are isomers. In total, the replication yield was 6.5 %. This is comparable to the 8.5 % replication yield when using magnetic colloids without a magnetic field. As the size and DNA functionalization was the same, comparable results are expected. In conclusion, while replicating sequences without magnetic alignment is not impossible, the cross-linking yields are so much lower that they become impractical.

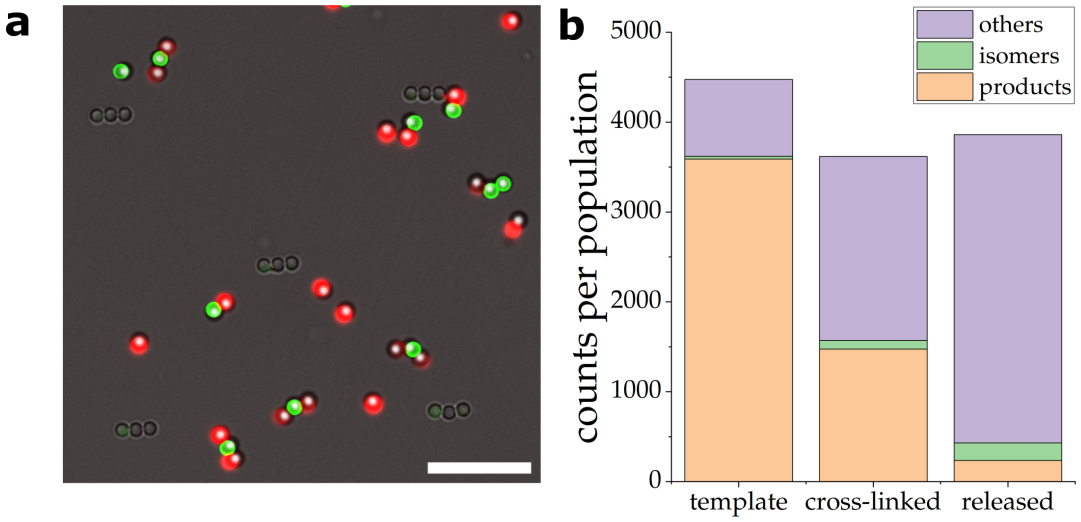

Figure S11: a) Microscope image of the released B'A'B' sequences made from silica colloids. Scale bars are 20µm b) Distribution of populations for the template, cross-linked and released states for BAB silica colloids.

3.3 Yield of re-binding on the primer sequences

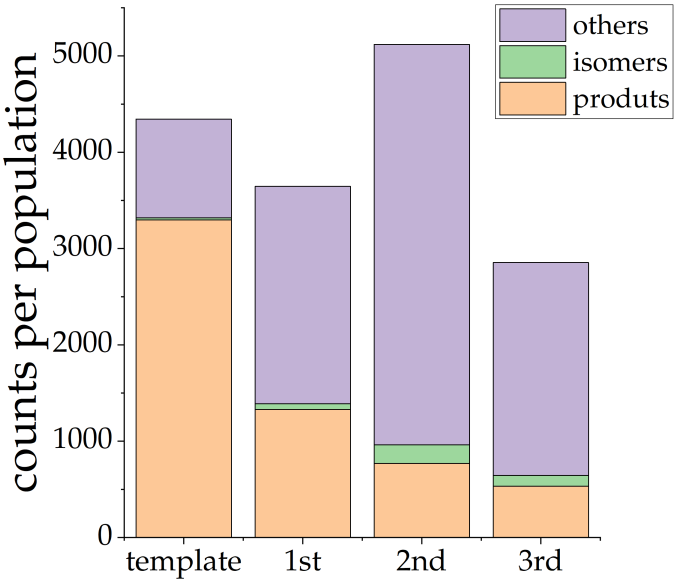

Figure S12: Counts of the different populations for the colloids on the template and the replicated colloids after the first 1st, 2nd, and 3rd time.

The possibility of reusing the same template was tested. Although technically possible, reusing the same template comes with various problems. The product yields in Figure S12 show that the yield decreases with every reuse. After the third time binding the colloids, only 40 % of the number of products of the first replication cycle was present. Moreover, from time to time, A' and B' monomer colloids were not only sticking to the template colloids but also to the PS-coated glass slide. This is why the total number of colloids increases for the second binding, as some of them counted as dimers because they were so close together, even though they were outside of the template area. This was not happening in the 3rd binding, where the total number of colloids was again lower. Another flaw in reusing the template was the more difficult release of the top complementary particle sequence with every cycle. Although possible, it required applying mechanical vibration for longer times, sometimes combined with flow.

3.4 Yield of the 3-particle multi-material clusters

Here, we quantify the yield of magnetic-silica-magnetic multi-material clusters. Based on the BAB replication, magnetic colloids were used for the B' colloids, and silica colloids were used for the A' colloids. As shown in the main manuscript, replication is possible. The counts per population and state are summarized in Figure S13. A share of 5.9 % of the product was present in the end. The replication efficiency of 6.6 % was again comparable to pure silica replication and the replication of magnetic colloids without using a magnetic field. This efficiency range seems to represent a general yield for a three-colloid system without the ability to align them.

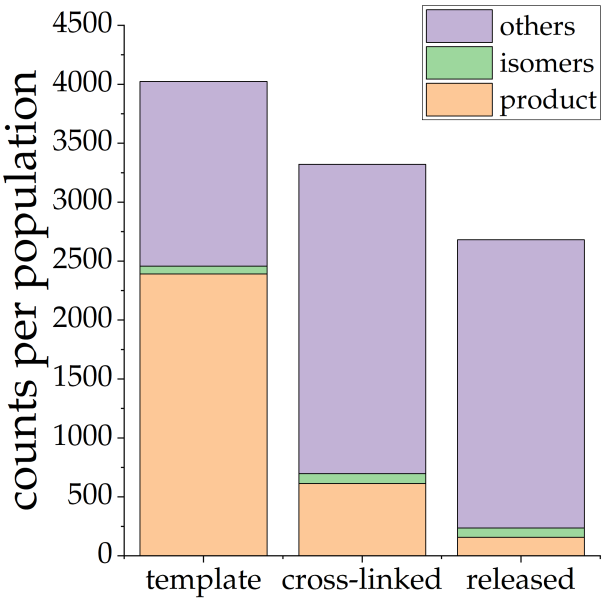

Figure S13: Counts of the different populations of sequences on the template, in the cross-linked state, and after release for magnetic-silica-magnetic colloidal sequences.

3.5 Yield of the 4 and 5-colloid sequences

In Figure S14a, the template for the BABA sequence is shown, while Figure S14b shows some replicated B'A'B'A' sequences. The counts per population for the sequences on the template, after cross-linking, and released can be found in Figure S14c. On the template, only 33 % of products were present, which then decreased to 16 % for the cross-linked state and to 15 % after the release. This gives a replication efficiency of 40 %, which is only a little lower than the replication efficiency for the BAB trimer. This is a good result considering that all the mechanisms proposed for explaining a yield decrease are amplified for a more extended sequence.

The BABBA sequence is investigated as an example of a five-colloid sequence. The template colloids are shown in Figure S14d, and some replicated and released colloids can be found in Figure S14e. The counts per population are shown in Figure S14f. The replication efficiency, in this case, was again roughly 40 %.

3.6 Replication of the square colloidal clusters and of sequences of 1.3 µm colloids

The replication of square shapes and smaller colloids is much less effective than in the other cases. We do not precisely quantify the yields but show representative microscopy images instead (Figure S15).

sCAPA does not only allow the production of linear colloid sequences. Non-linearly shaped colloidal assemblies such as triangles or squares were also feasible, with examples of released squares shown in Figure S15a. Only a few clusters could be successfully replicated. No magnetic field was used for these colloids, as applying a magnetic field led to repulsion orthogonal to the magnetic field. But without the magnetic field, as previously discussed, only a small fraction of assemblies had particles in direct contact.

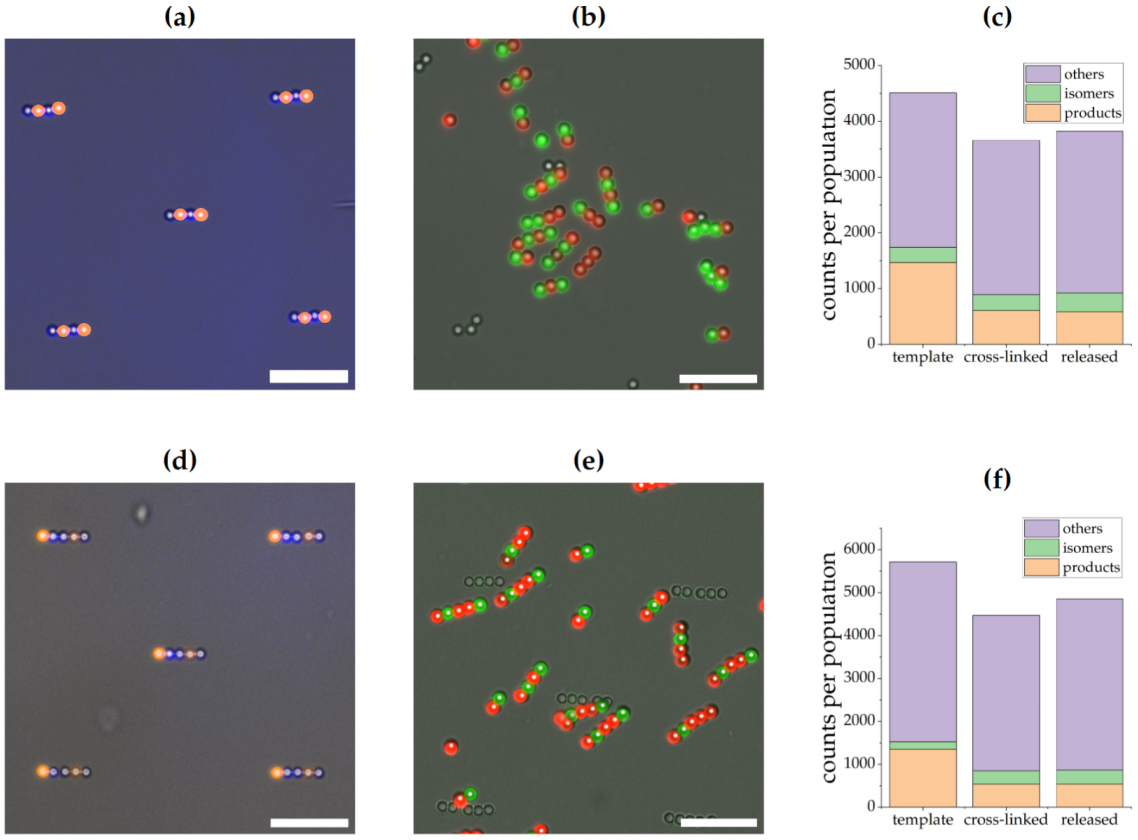

Figure S14: Microscopy images of BABA silica colloids on the template (a) after release(b). (c) Distributions of the populations of sequences on the template, after cross-linking, and release for BABA colloidal sequences. Microscope image of BABBA silica colloids on the template (d) after release(e). (f) Distributions of the populations of sequences on the template, after cross-linking, and release for BABBA colloidal sequences. Scale bars are 20 µm.

A different monomer colloid size is of interest to investigate the replication process's capabilities and robustness. For this purpose, 1.3 µm sized colloids were investigated. Our process flow is also applicable to these smaller particles, as shown in Figure S15, where the complementary colloids are bound and cross-linked. As the smaller colloids are lighter than the 2.7 µm colloids, they hovered at a greater distance from the template, reducing the binding rate. To prevent swirling up these smaller and lighter colloids, the pulling speed was decreased to $1\,\mathrm{um/s}$ during the binding, but still, the binding was less effective than for the larger colloids.

However, as demonstrated in Figure S15b, the main issue for the small colloids was the release. While a few colloids were released via mechanical vibration, most remained stuck to the template. We hypothesize it is easier for the smaller colloids to cross-link to the primer sequence, and therefore, an alternative crosslinker is needed to scale this process down to smaller colloids.

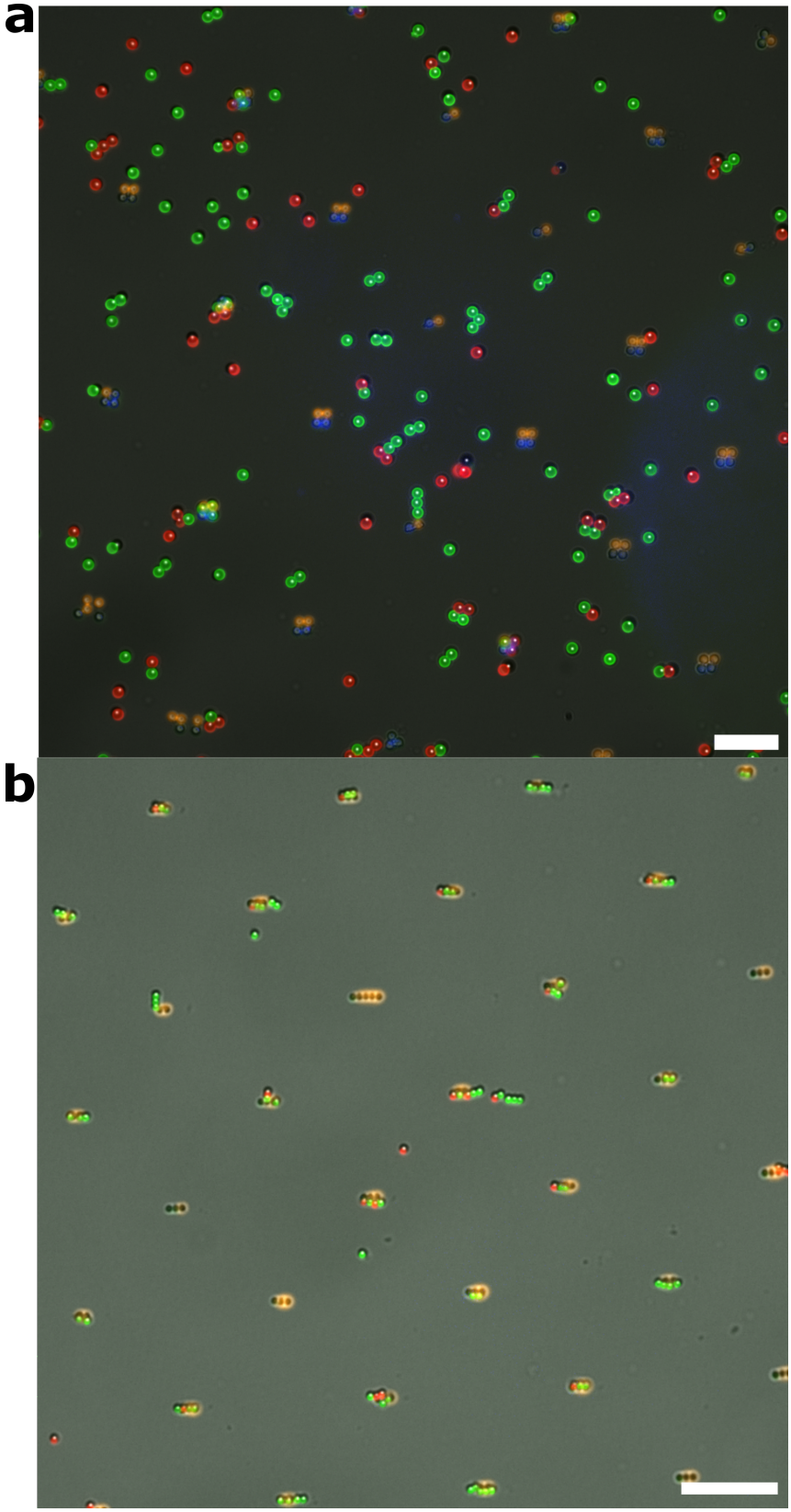

Figure S15: Microscopy images of square BBAA shapes (a) and 1.3 µm BAA sequences after release. Scale bars are 20 µm.

4 Alternative cross-linking approaches

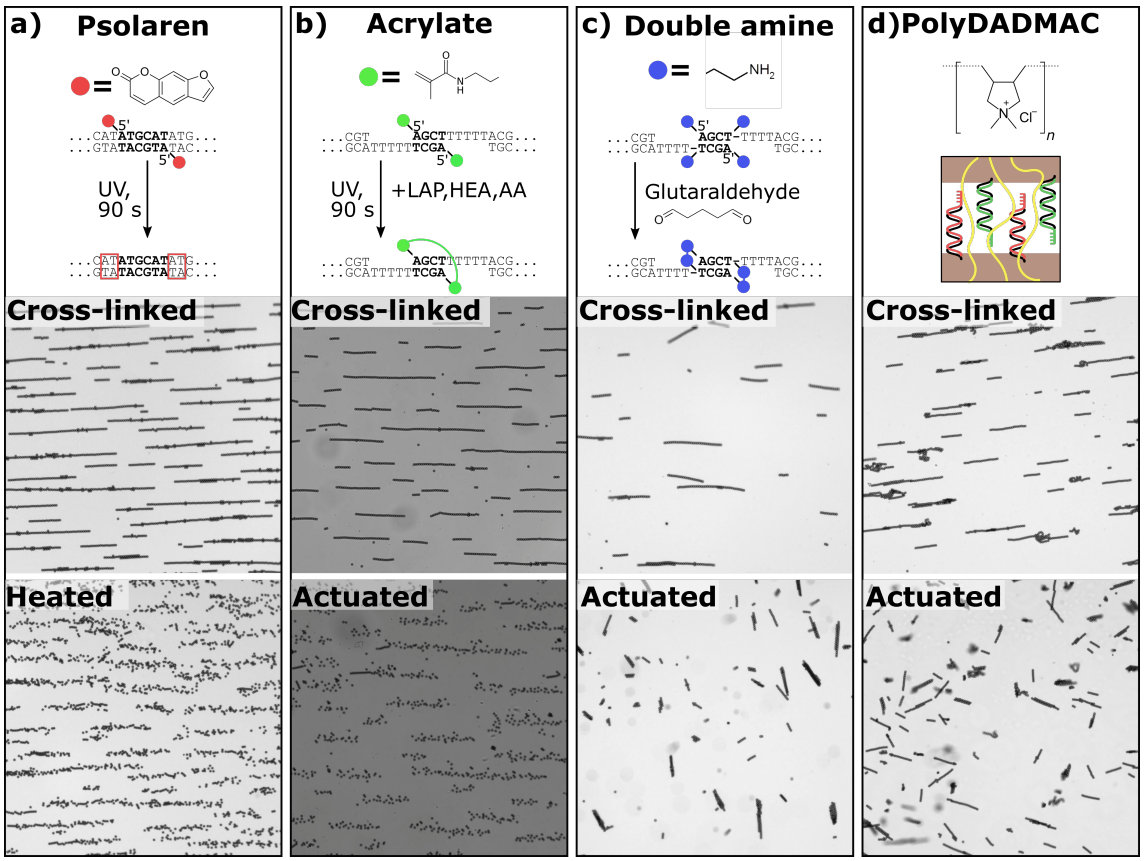

Figure S16: **Alternative cross-linker designs** Each panel describing a cross-linker consists of three parts; a schematic of the design of the cross-linker and cross-linking procedure (top), a brightfield micrograph of the cross-linked magnetic colloidal chains (middle), and the same cross-linked colloids after heating to 50 °C (for a) or mechanical actuation (for b-d) (bottom). a) Cross-linking using palindromic DNA with UV-cross-linkable psolaren. b) Cross-linking using palindromic DNA with acrylate groups in a photopolymerizable medium. c) Cross-linking using palindromic DNA with two amines and adding glutaraldehyde. d) Cross-linking using large cationic polyDADMAC.

Cross-linking the colloidal sequences has been one of the major challenges of this work. We went through a few iterations of cross-linker design and would like to share this process as it might be useful for others developing cross-linking approaches. The cross-linkers we tested can be grouped into four categories:

- Palindromic DNA with UV-cross-linkable psolaren
- Palindromic DNA with acrylate groups in a photopolymerizable medium
- Palindromic DNA with two amine groups bridged with glutaraldehyde
- Large cationic polyelectrolyte

In the following paragraphs, we will briefly discuss these designs and the most promising results we obtained from them. The colloids were functionalized with the same protocol as described in the methods, but 25 % of the normal DNA was replaced with the cross-linker in the

case of the palindromic DNA-based cross-linkers. To experimentally screen the cross-linkers, we assembled magnetic colloids into chains with a magnetic field in the suspension buffer. We subsequently cross-linked the colloids. We then subjected the sample to temperatures above 50°C and/or mechanical actuation to determine whether the colloidal chains were robustly cross-linked.

Palindromic DNA with psolaren: Our first design, palindromic DNA with psolaren, was based on existing literature [3]. In this design, the colloids are coated with a second type of DNA with a self-complementary sticky end, also known as a palindrome. At the end of this sticky palindrome, there is a psolaren end-group that can cross-link DNA when illuminated with UV light. This approach is elegant because it selectively cross-links the DNA by illuminating it with UV light without the need for additional chemicals. By using different palindromes, we can ensure no cross-linking between the template and the complementary sequence.

We experimented with different designs, including DNA sequences with palindromes ranging from 4-6 base pairs in length, the presence of a short poly-T spacer between the backbone and the sticky end, and psolaren end groups (provided by EuroGentec) with and without a short PEG spacer.

The most promising design was a six-base pair palindrome without poly-T or PEG spacers that we cross-linked by exposing it to UV light for 90 seconds at 365 nm. However, with this design, we observed that some smaller clusters stayed intact even after heating above the melting temperature of 50°C, as shown in Figure S16a, but these clusters were easily broken by mechanical force. These results did not show enough promise to continue with this cross-linker.

Palindromic DNA with acrylate groups: The second design also uses a palindromic sticky end with a different cross-linking method. In this design, we use two acrylate end groups (Acrydite, IDT) with a medium containing acrylate monomers and a photo-initiator. When exposed to UV light, the monomers polymerize, and the growing polymer chains bridge the two acrylates between the polymers. This design has a large parameter space, including the design of the DNA sequences and the choice of specific monomers, photo-initiators, and concentrations.

The most promising design used a four-base pair palindrome with a poly-T spacer and a medium containing LAP, HEA, and AA in the suspension buffer, cross-linked by a 90-second exposure at 365 nm. With this design, the cross-linked chains remained intact even after heating to 50°C. However, the polymerization strongly increased the viscosity of the medium, and the colloidal chains were still easily broken by mechanical actuation, as shown in Figure S16b.

Palindromic DNA with two amines: The third major design still utilizes palindromic DNA, but instead of light activation, we chose to use a simpler chemical approach by adding a chemical agent as a cross-linker after the clusters were assembled. The DNA-sequences contain two primary amines, one at the end of the DNA sequence and one inner-chain amine at the beginning of the sticky palindrome (provided by MicroSynth). This configuration ensures the amines are in close proximity when the palindromes are hybridized. Glutaraldehyde is used as a chemical cross-linker for the amines.

We observed strong cross-linking when adding 1% glutaraldehyde, resulting in colloidal chains that survived heating and mechanical actuation, as shown in Figure S16c. However, this cross-linking also occurred with control colloids that did not contain the double amine palindrome, and it strongly bound the complementary colloids to the template, making release impossible. This suggests that a secondary non-specific reaction occurs between the glutaraldehyde and the colloids. When we used a lower 0.1% glutaraldehyde concentration, we observed no cross-linking of colloids with and without the palindrome, and the chains were easily broken with heat or mechanical actuation.

Large cationic polyelectrolyte: After facing challenges with the palindromic DNA design, we pursued an entirely different route. The non-specific cross-linking of the glutaraldehyde seemed robust and easy. However, because glutaraldehyde is a small molecule, it cross-links ev-

erywhere, making it difficult to release the complementary colloids from the template. Therefore, we explored using 450 KDa polyDADMAC ($R_h \approx 80$ nm) as a larger non-specific cross-linker to overcome this issue. The cationic polyDADMAC cross-links with the anionic DNA via electrostatic interactions, forming a complex coacervate-like structure. This larger cross-linker is more selective than glutaraldehyde because it cannot easily reach the connection between the template and complementary colloid. We observed very robust structures that cannot be broken with heat or mechanical actuation when polyDADMAC was added to the colloids, as shown in Figure S16d. We believe this cross-linker is so effective because it has much more interactions than palindromic DNA, which can only provide a few thousand bonds at most.

5 Details on the release

5.1 Heating versus mechanical actuation

We compare the difference in release between heating and mechanical vibration as follows; We started with a standard template of single A colloids sunk into PS, bound the A' magnetic colloids on top, and removed most unbound colloids. This sample was the put on a heating stage (Linkam) at 70 °C for 10 minutes. The release particles were counted by subtracting the before and after images, and we observed that 15 % of the colloids were released by heating (Figure S17 top). We used a similar sample and applied mechanical vibration by placing a toothbrush without the brush head (Oral-B, 106 Hz, 0.7 mm displacement) for approximately 10 s on the glass slide. We again compared the images before and after mechanical actuation and observed that 95 % of the particles were released (Figure S17 bottom). Some alignment of the magnetic colloids was present due to the metal heating stage.

5.2 Characterization of the toothbrush's vibrations

The frequency and amplitude of the toothbrush, used for mechanical actuation to release the colloids, were determined with a high-speed camera (Photron, FastCam Mini Ax). The toothbrush was filmed from the side at 500 and 5000 fps with strong illumination from the back. We observed that the toothbrush rotated back and forward with a maximum displacement of 0.7 mm at the tip at a frequency of 106 Hz (Figure S18).

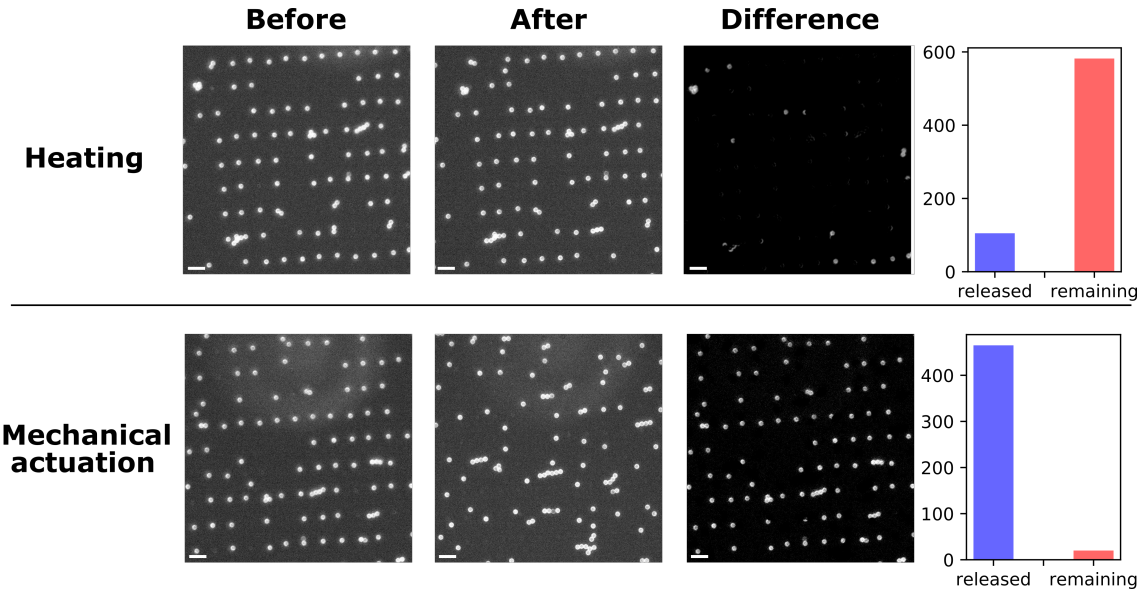

Figure S17: **Heating versus mechanical vibration.** The image panels show fluorescence micrographs of the A' colloids on a single A colloid template, before release(left), after release (middle), and the difference between the images showing all the release colloids (right). The top row shows the result of the heating procedure (10 min, 70 °C), and the bottom row shows the result of the mechanical vibration with the toothbrush. The plots show how many colloids were released (taken from a larger overview) and how many were still bound to the template colloids. The scale bars are 20 µm.

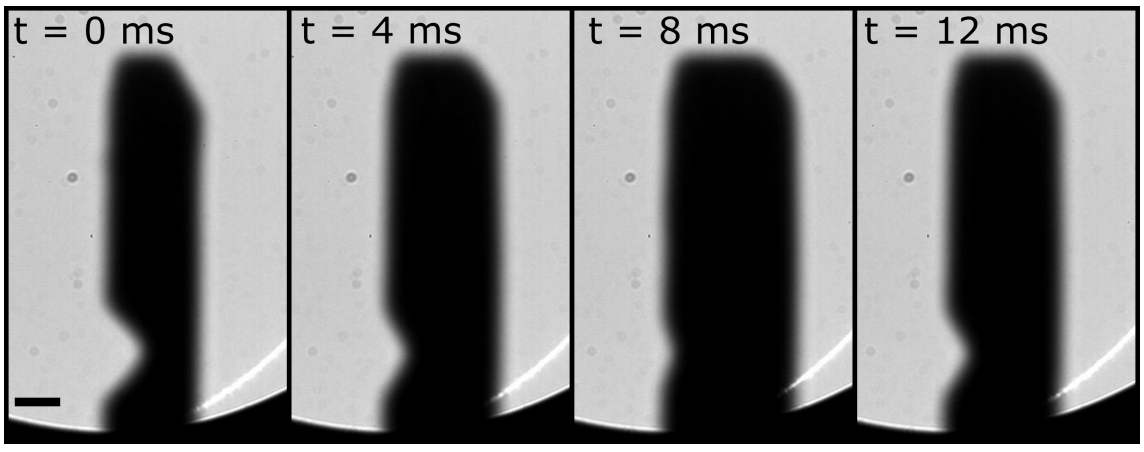

Figure S18: **Characterization of the toothbrush** The panels show four frames of the actuating toothbrush at 4 ms intervals from a high-speed movie at 500 fps. The scale bar is 1 mm.

6 Details on FACS

Although a purity of 49 % could be achieved after release, many unwanted byproducts were also harvested, i.e., removed from the cell, during the harvesting of the replicated colloids. The byproducts from harvesting came from monomers that got stuck at the sides of the replication cell and tubing. These monomers could also cross-link to aggregates and were also harvested. This led to a decrease in the harvested share of the product of 25 %, which is not favorable for further exponential growth cycles. Fluorescence-assisted cell sorting was used to purify the samples further. By using FACS, the purity could be increased up to 80 %. In our experiments, FACS could not distinguish between isomers, meaning every trimer consisting of two B' and one A' colloid, is considered a correct product. Nevertheless, FACS is more precise than sorting by size using magnetic fields or mechanical filters, as other trimers, such as B'B'B', were sorted. Fig. S19 shows two typical FACS plots. At the left one, each colloid is plotted according to its forward and side scattering amplitude. Bigger particles scatter more, and a given cluster size can be assigned to the clouds. On the right plot, each colloid is plotted according to its A' and B' fluorescent intensity. The clouds are numbered, and the images at the bottom show an example per cloud. Additionally, FACS can also be used to analyze different populations. The FACS data tells us that approx. 40 % were BAB clusters (or isomeric equivalents). Interestingly, this number is higher than the 25 % obtained from counting the particles in an aliquot. We suspect a part of the wrong colloidal clusters observed in the microscope was only weakly bound together and these clusters were broken up into single particles in the flow cytometer. The correct sequences on the other hand were strongly cross-linked and are more likely to survive the strong flows.

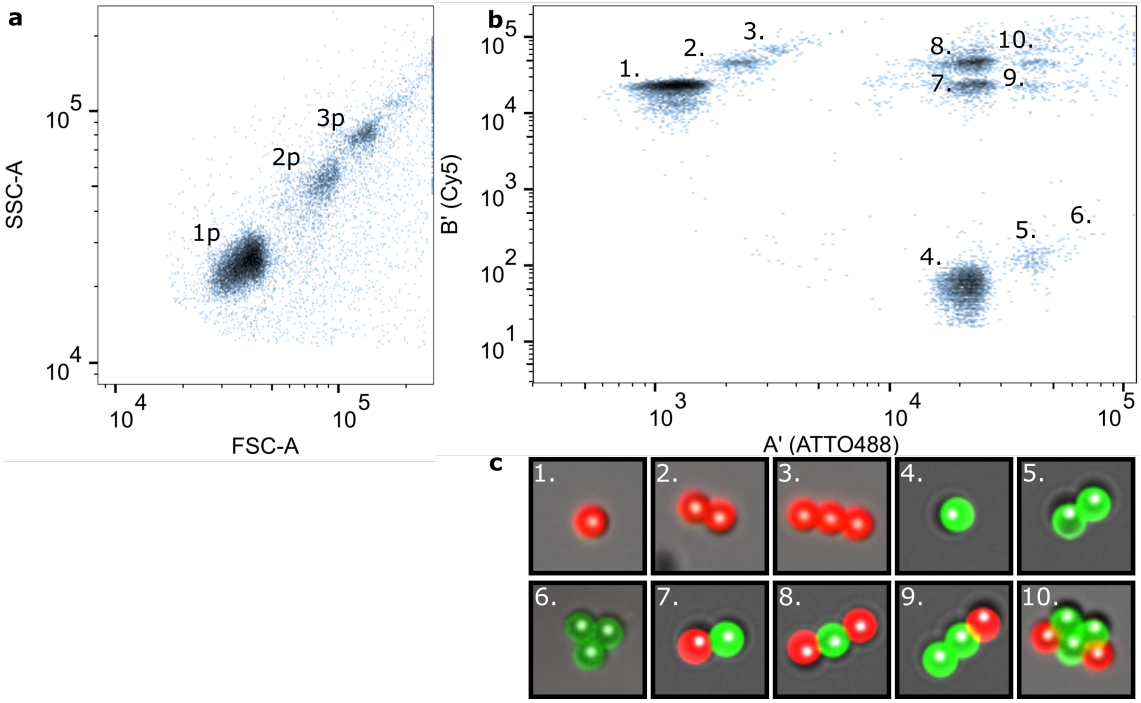

Figure S19: **FACS** All FACS data was obtained from a BAB replication. a) Forward scattering area (FSC-A) and side scattering area (SSC-A) of the colloids and colloidal cluster, showing three clear data clusters corresponding to single monomers (1p), two-particle clusters (2p), and three particle clusters (3p). b) FACS scatter plot showing the Cy5 and ATTO488 fluorescence intensities including the monomers. The numbers 1-10 correspond to colloidal clusters with different compositions that can be found in our samples at the different data clusters. c) Examples of the different colloidal clusters corresponding to the numbers in (b).

7 Details on the patchy copy sequences and second generation binding

7.1 SEM-EDX investigation of patchy copy sequences

We used SEM of the nanoparticle-coated colloidal sequences to show the presence of patches coming from the contact point between the template and complementary colloids. Some sequences were deliberately not released to ensure we could trace back the colloidal sequences that originated from a template. We flushed the microfluidic chip with EtOH to take it apart without releasing the sequences. We manually removed the sequences from the templates with a micromanipulator (IMINA Technologies, MICRO miBot). Smooth patches of around 600 nm in diameter on a rough colloid surface were then observed with SEM on both the template and the copy sequence (Figure S20a-b), which indicates that the nanoparticles selectively blocked part of the surface. We observed that the complementary sequences made from the SiO_2 colloids almost always broke during the manual release due to their weak cross-linking. We also had the same patches on colloidal sequences released in suspension, but these tended to aggregate during sample drying (Figure S20c).

We used 2.7 µm SiO_2 instead of magnetic colloids to visualize the patches. We tried to observe the patches on the magnetic Dynabeads, which had a stronger cross-linking, so they were released intact with the micromanipulation. However, these colloids have a rougher surface, and more uneven shape, making the topological contrast between the patch and the nanoparticles-coated hard to distinguish (Figure S20d). We used energy-dispersive X-ray spectroscopy (EDX) mapping to see that the colloidal sequence is covered with SiO_2 (Figure S20e-f), which was not present in the bare Dynabeads. This confirmed that the magnetic colloids were covered in nanoparticles similar to the smooth SiO_2 colloids. However, we needed to use a high acceleration voltage of 15 KeV to obatin enough signal for the EDX mapping, resulting in a high penetration (¿ 1 µm), making it impossible to conclusively confirm the small patches with this approach.

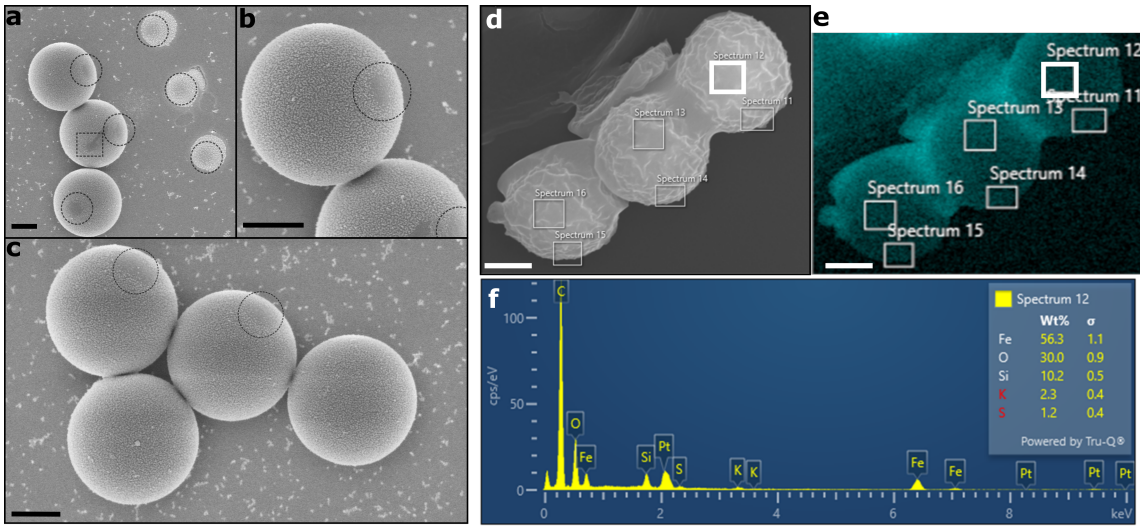

Figure S20: **SEM and EDX of patchy copy sequences** Panels a-c are SEM micrographs of 8 nm SiO_2 nanoparticles on 2.7 µm SiO_2 colloids with empty patches where the particle was bound to the template. The circles indicate the patches. a) An BAB colloidal sequence with one colloid detached and a scratch caused by removing the sequence from the template (indicated by the square) b) A zoom-in of the panel "a.". c) A larger overview image of the patchy colloids shown in the main text. d) SEM micrographs of 8 nm SiO_2 nanoparticles on 2.7 µm Dynabead magnetic colloidal sequence. e) EDX mapping of the Si signal corresponding to the image in panel d. The thick white square indicates the local spectrum shown in f. f) EDX spectrum of nanoparticle-coated magnetic colloids in the area shown in panel e. The scale bars are 1 µm.

7.2 Overview of the second-generation binding

After coating with the nanoparticles, we released the colloidal sequences from the primer and added the complementary colloids. In this case, the complementary colloids were the A and B colloids that, usually are the colloids of the primer. We noticed that the nanoparticle-coated copy sequences stuck significantly more to the PS substrate than standard colloidal sequences, and the release was not as effective. There was still some non-specific aggregation, partly because we used a magnet to collect the monomer colloids and nanoparticle-coated sequences. Fortunately, we did find examples of selective directional binding (S21). Unfortunately, the current cross-linking method cannot selectively cross-link if both sequences are in suspension. Therefore, the exponential replication process was halted at this step, and more work is needed to improve this process. Nevertheless, these preliminary results demonstrate selective binding to a second-generation template, a crucial step toward future exponential replication.

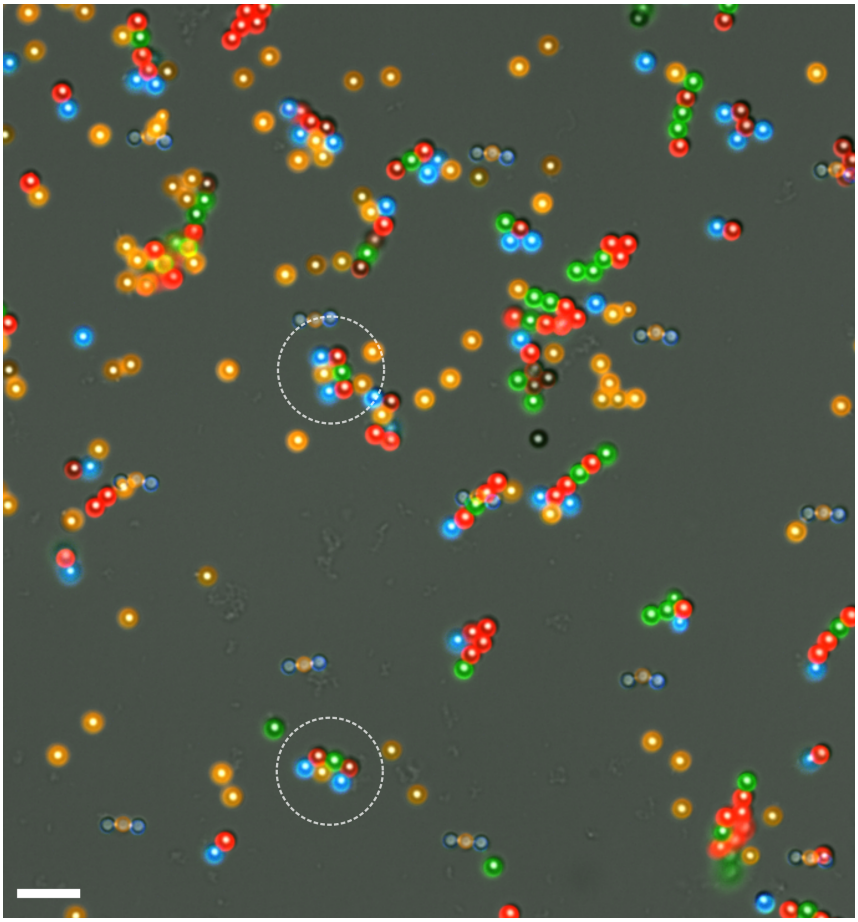

Figure S21: **Overview of the second-generation binding.**

8 Suppporting Movies

- **SI Movie 1**: Movie of the complementary colloids flowing over the primer sequences. The primer sequences and colloids that are caught binding are highlighted. The movie is sped up 1.5 times.
- **SI Movie 2**: Movie of the magnetic complementary colloids bound to primer sequences

under the influence of a magnetic field. During the movie, the magnetic field is slowly increased and then turned off.

References

[1] Cailing Hou, Linxia Zhang, Yue Wang, and Zhimin Wang. Synthesis and application of streptavidin functionalized organosilica microparticles. *Journal of Applied Polymer Science*, 132(9):1–10, 2015.

[2] Steven van Kesteren, Laura Alvarez, Silvia Arrese-Igor, Angel Alegria, and Lucio Isa. Self-propelling colloids with finite state dynamics. *Proceedings of the National Academy of Sciences of the United States of America*, 120(11):1–9, 2023.

[3] Mirjam E. Leunissen, Rémi Dreyfus, Roujie Sha, Tong Wang, Nadrian C. Seeman, David J. Pine, and Paul M. Chaikin. Towards self-replicating materials of dna-functionalized colloids. *Soft Matter*, 5:2422–2430, 2009.

[4] Songbo Ni, Jessica Leemann, Heiko Wolf, and Lucio Isa. Insights into mechanisms of capillary assembly. *Faraday Discussions*, 181:225–242, 2015.

[5] Daniel B. Allan, Thomas Caswell, Nathan C. Keim, Casper M. van der Wel, and Ruben W. Verweij. soft-matter/trackpy: Trackpy v0.5.0, 2021.